A seasonal circulation index for the ocean and its application to the South China Sea

Qiang Li[1,2,3], Run Xin Huang[4] and Lingling Xie[1,2,3]*

[1]Department of Marine Science, College of Ocean and Meteorology, Guangdong Ocean University, Zhanjiang, China, [2]Key Laboratory of Climate, Resources and Environments in Continent Shelf Sea and Deep Ocean (LCRE), Zhanjiang, China, [3]Key Laboratory of Space Ocean Remote Sensing and Applications (LORA), Ministry of Natural Resources, Beijing, China, [4]Department of Physical Oceanography, Woods Hole Oceanographic Institution, Woods Hole, MA, United States

Ocean circulation is crucial in redistributing mass and energy on Earth. However, it varies significantly on a seasonal time scale due to external forcing. To quantify the seasonality of ocean circulation, we propose a seasonal circulation index (*SCI*). This index is defined as the normalized maximum deviation from the velocity vector, whose magnitude is the largest in one period. We have substantiated the efficiency of this index using the monsoon wind in the South China Sea (SCS). By utilizing this index, we have obtained the 3D structure of the seasonality of ocean circulation in the SCS. The *SCI* and the seasonal circulation amplitude (*SCA*) exhibit large values over 0.9 and 0.8 m s^{-1} in the western boundary current. Alternating southwest-northeastward bands of *SCI* with high and low values are distributed from the north shelf to the south, especially in the eastern basin. Although *SCA* decreases significantly with depth, *SCI* exhibits values higher than 0.7 in both the middle and deep layers, indicating a noteworthy seasonality and middle-layer enhancement in the abyssal basin of the SCS.

KEYWORDS

seasonal circulation index, deep circulation, South China Sea, monsoon, belt-like strucuture

1 Introduction

A significant seasonal cycle exists in many regions of the world's oceans (Liu and Zhou, 2020; Phillips et al., 2021). Therefore, an efficient method to study this phenomenon is desirable. The South China Sea (SCS) is an example since it is located in the East Asian monsoon corridor, where northeasterly winds prevail in boreal winter and southwesterly winds in summer (Liu et al., 2008). The seasonal variation of the upper ocean circulation in the SCS has been well documented (Wyrtki, 1961; Wang et al., 2003; Hu et al., 2020). Additionally, the Kuroshio intrusion and mesoscale disturbances from the Pacific Ocean penetrate the Luzon Strait (LS) into the SCS (Zheng et al., 2011; Xie et al., 2016). Moreover,

the SCS throughflow (SCSTF) flows through the SCS, creating a passage from the Pacific Ocean to the Indian Ocean (Qu et al., 2006; Wei et al., 2019).

The SCS monsoon (SCSM), an essential driver of ocean circulation, has received considerable attention (Jiang et al., 2006; Liu and Zhu, 2021). Researchers have proposed quantitative monsoon indexes to describe the switch and seasonal variability of the winds over the SCS (Wang et al., 2009; Zhou et al., 2018). With the SCSM index (SCSMI), the onset date and strength of the summer monsoon over the SCS can be identified (Mao and Wu, 2007; Kajikawa and Wang, 2012). Additionally, researchers have revealed the various modes of the SCSM and their relationship with other processes, such as El Niño and Southern Oscillation and the COVID-19 events (Yim et al., 2014; He et al., 2022).

The advancements in *in-situ* observation, remote sensing, and numerical simulation have enabled more detailed insights into the seasonal circulation in the SCS. According to Hu et al. (2000), the anticyclonic summer circulation in the southern SCS (SSCS) reverses to become cyclonic in winter, while the cyclonic circulation in the northern SCS (NSCS) remains due to disturbances from the Pacific. In recent years, there has been increasing attention on the basin circulation in the middle and deep layers of the SCS (Wang et al., 2011; Tian and Qu, 2012; Cai et al., 2020; Zhu et al., 2022). Gan et al. (2016) demonstrated a climatological cyclonic-anticyclonic-cyclonic (CAC) three-layer circulation in the SCS, with a seasonally reversed circulation in the upper layer. Moreover, recent studies have suggested seasonal variation in the deep-layer ocean circulation in the SCS (Liu and Lan, 2022; Zhu et al., 2022).

Although the seasonal variations in ocean circulation in the SCS have been recognized, no quantitative index is currently available to represent this variability accurately. In contrast to the various studies on the SCS monsoon index, developing an improved index to describe seasonal ocean circulation is necessary. A quantified index can aid in interpreting not only the circulation itself but also climate and environmental changes related to it. Therefore, in this study, we propose a new index, the Seasonal Circulation Index (*SCI*), to quantify the strength of the seasonality of large-scale ocean circulation. This paper is organized as follows: Section 2 presents the data and methods used in the study. Section 3 outlines the definition of the SCI and its validity in the SCS monsoon. Section 4 provides a detailed description of the *SCI* of ocean circulation in the SCS, and Section 5 presents our discussion and conclusions.

2 Data and methods

2.1 Surface wind data

The wind data used in this study is based on the monthly 10-meter sea surface wind velocity from ERA5, which was obtained from https://cds.climate.copernicus.eu/. The data has a spatial resolution of 0.25 degrees by 0.25 degrees and covers the period from 1979 to the present.

2.2 Ocean current data

We use monthly current velocity data from the Simple Ocean Data Assimilation (SODA, http://apdrc.soest.hawaii.edu/datadoc/soda_3.3.1.php) reanalysis for ocean calculations. The SODA data has a horizontal resolution of 0.25°, suitable for investigating large-scale circulation, and consists of 50 vertical layers from the surface to 5500 m. The data covers the period from 1980 to 2015 and has been extensively used in previous studies on the circulation of the SCS (Wang et al., 2006; Fang et al., 2012; Lan et al., 2015).

Figure 1 shows the comparison of the winter and summer SSH and surface current velocity from the two datasets in the SCS. One can see that the two data sets have similar large-scale distribution characteristics, that is, the SSH in the north and west of the basin is generally lower than that in the east and south. In winter (Figures 1A, C), both data sets show cyclonic circulation with the lowest SSH east of the Luzon Strait. In summer (Figures 1B, D), anticyclonic circulation appears in the southern basin and the surface current velocity gets slower than that in winter. The northeastward jet near the Vietnam coast is evident in both of the datasets. The similarity further indicates the efficiency of the SODA data in studying the ocean circulation in the SCS.

2.3 SCSMI

The SCSMI used in this study is based on the method suggested by Wang et al. (2004), which involves averaging the 850 hPa zonal wind over the region of 3.75°N – 16.25°N and 108.75°E – 121.25°E in August. This index is commonly used to identify the onset of the summer monsoon and quantify the intensity of the SCSM.

3 SCI and application in the SCSM

3.1 Seasonal circulation index and seasonal circulation amplitude

To emphasize the transition of current direction, the dominant direction should be the first choice of the research object, which is reflected by the strongest scale of wind or current velocity in one year, that is,

$$w_0 = (u(m_0))^2 + (v(m_0))^2 \qquad (1)$$

where (u, v) denotes zonal/meridional components of wind or current velocity, and m_0 is the month when wind/current velocity is maximum. The current velocity in the other months is considered in the form of the inner product with that in the month m_0, that is,

$$w(m) = u(m_0)u(m) + v(m_0)v(m), m = 1, 2, …, 12 \qquad (2)$$

where m denotes the month. This form includes the peak month denoted in Eq. (1), and depicts the deviation from the dominant velocity, both in scale and direction. In fact, $w(m)$ can also be written in the following form
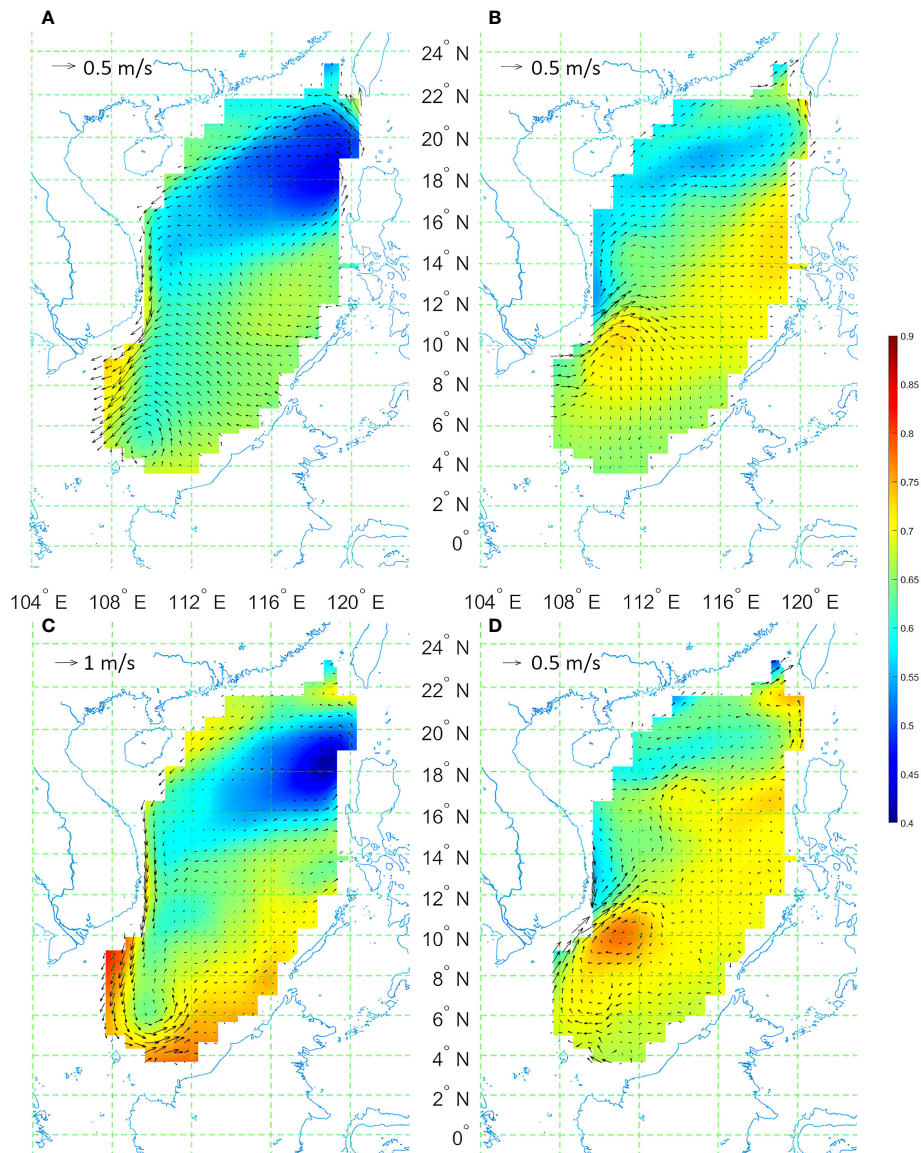
FIGURE 1
2D distribution of winter **(A, C)** and summer **(B, D)** SSH (color, in m) and surface velocity (quiver, in m s^{-1}) from SODA data **(A, B)** and AVISO satellite observations **(C, D)** in the SCS.

$$w(m) = |\mathrm{u}(m_0)||\mathrm{u}(m)| \cos <\mathrm{u}(m_0), \mathrm{u}(m)>, m = 1, 2..., 12 \quad (3)$$

Where $\mathbf{u}=(u,v)$, and $<\mathbf{u}(m_0),\mathbf{u}(m)>$ is the angle between velocity vectors in two month.

The Seasonal Circulation Index (*SCI*) is defined as

$$SCI = \max\left(\frac{w_0 - w(m)}{2w_0}\right) \quad (4)$$

which reflects the normalized maximum extent of the deviation in one year, indicating the seasonal overturning of velocity, which varies from 0 to 1. When *SCI*=0, the current's direction, and amplitude remain unchanged over the whole year; when *SCI*=1, the orientation of the most deviated vector turns 180 degrees, and the amplitude remains the same. *SCI*=0.5 means that the projection of the extreme deviated velocity to the maximum velocity is zero; either the deviated velocity is zeros or perpendicular to the maximum

velocity. The *SCI* emphasizes the seasonal reversal of current in a normalized way, but it does not include important information related to the amplitude of the seasonal cycle; thus, another index is needed to describe the variability in the amplitude. Here we propose Seasonal Circulation Amplitude (*SCA*) as

$$SCA = \sqrt{\max(w_0 - w(m))} \quad (5)$$

which is the square root of the denormalized form of *SCI* and whose dimension is the same as that of velocity.

In this paper, we derive the climatological *SCI* from climatological monthly velocity rather than long-term averaged yearly *SCI* based on monthly velocity in that year. The two results of *SCI* indexes are similar to each other both in pattern and value, indicating the robustness of *SCI* in the application.
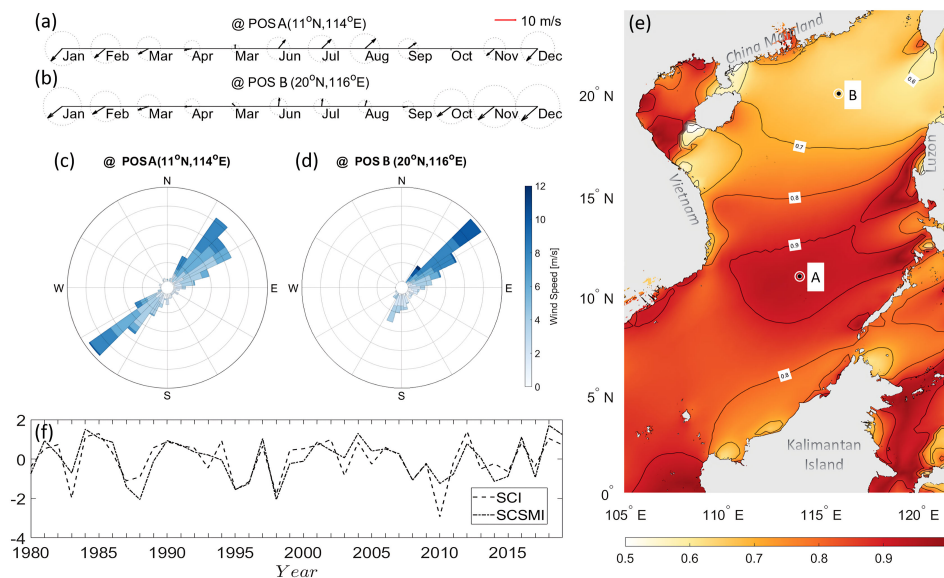
FIGURE 2
Climatological monthly wind vectors **(A, B)** and wind roses **(C, D)** at station A **(A, C)** and B **(B, D)**, respectively. **(E)** 2D (x-y) distribution of climatological SCI_w over the SCS. **(F)** Time series of the normalized yearly SCI_w (dashed line) in the central SCS and the normalized SCSMI (dotdashed line).

3.2 Application of *SCI* in SCSM

The *SCI*, as defined above, is first applied to wind data, denoted as SCI_w. Figure 2 illustrates the annual cycle of surface winds and the distribution of climatological SCI_w in the SCS. As shown in Figures 2A–D, the surface winds at two stations in the SCS undergo changes in both magnitude and direction from northeasterly to southwesterly over a year. At station A in the SSCS (11°N,114°E, Figure 2E), the maximum wind magnitude w0 occurs in January, while the most deviated wind occurs in August (Figure 2A). The wind directions in these two months are almost opposite, but the magnitudes are similar. The SCI_w at station A is 0.93 (Figure 2E), close to 1. At station B in the NSCS (20°N,116°E, Figure 2E), the wind reaches its maximum magnitude in December and has the most deviated direction in August (Figure 2B). However, the magnitude of wind in August is only half of that in December. Thus, the SCI_w at station B should be smaller than the SCI_w at station A. As shown in Figure 2E, the SCI_w at this station is only about 0.6. The SCI_w values reflect the extent of the wind variation, both in magnitude and direction. This result is also supported by the wind rose at stations A (Figure 2C) and B (Figure 2D).

The SCI_w values are generally above 0.7 in most areas of the SCS, with large values reaching around 0.9 in the southern basin and smaller values around 0.6 in the north (Figure 2E). The basin-wide mean SCI_w is over 0.8, indicating strong seasonality of the SCSM (i.e., the wind direction nearly reverses in the annual cycle). A zone with high SCI_w values (>0.9) is observed in the SSCS (9°N – 12°N, 111°E – 116°E), where the SCSM dramatically reverses from northeasterly in winter to southwesterly in summer.

Figure 2F depicts the time series of the normalized SCSMI (revised from Wang et al., 2004) and yearly SCI_w in the central SCS (3.75°N – 16.25°N, 108.75°E – 121.25°E) where SCSMI is defined.

The graph indicates that both time series show similar interannual variation trends, with a high correlation coefficient of 0.81 (p<0.01), further supporting the effectiveness of SCI_w in representing the seasonal variation of wind velocities and providing a simple index to quantify the SCSM. The normalized SCSMI and SCI_w even have similar values in most years, while significant differences appeared in some years such as 1983 and 2010. In fact, the SCSMI is related to the zonal wind in summer while SCI_w represents the deviation of summer wind from the strongest wind in winter. The enhanced westerly wind in the southwestern SCS increases the SCSMI in 1983 and 2010, while SCI_w keeps low value under the SCSMI.

The SCI_w not only effectively quantifies the intensity of the SCSM but also helps identify the critical area for calculating the SCSMI. Previous studies have used varying meteorological parameters and definition areas for the SCSMI, with some indicators being subjective or controversial. In this study, the distribution of SCI_w above 0.9 in Figure 2E was used to narrow the definition area to 9-12°N and 111-116°E (Table 1). This approach identifies the most active region for the onset of the summer monsoon.

4 *SCI* of the ocean circulation

In this section the SCI is applied to the ocean current, and it is denoted as SCI_o. We will discuss both the horizontal and vertical distribution of SCI_o in the SCS.

4.1 Horizontal distribution

Figure 3A illustrates the SCI_o of the surface ocean current velocity climatology in the SCS. In contrast to SCI_w, SCI_o of the
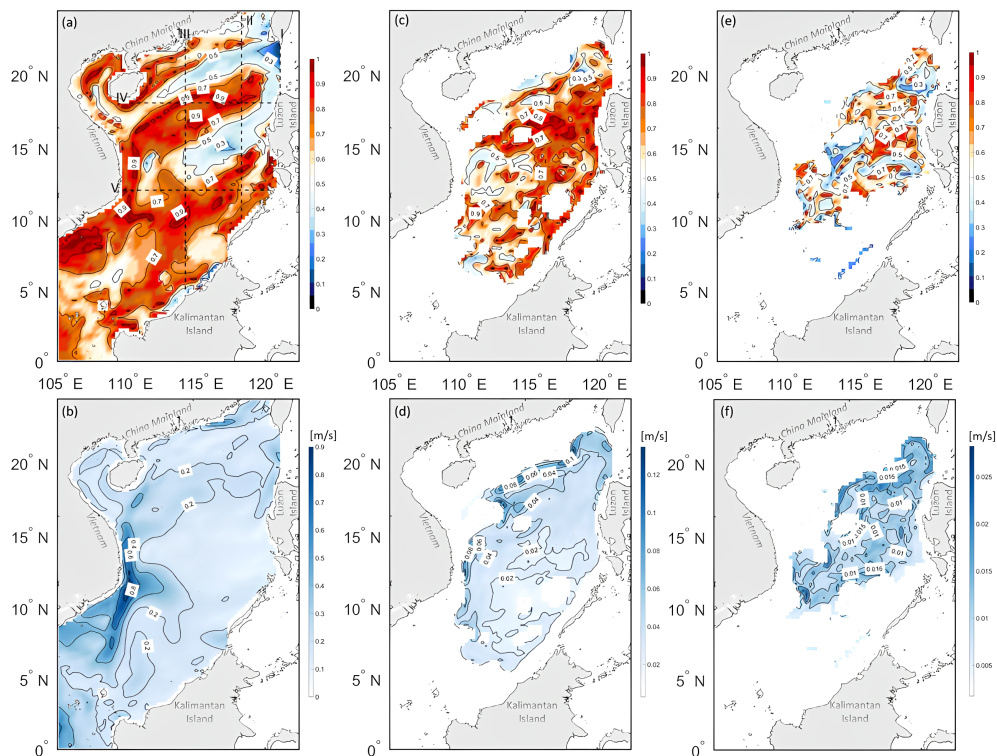
FIGURE 3
SCI_o **(A, C, E)** and SCA_o **(B, D, F)** of climatology current in three different layers of the SCS. **(A, B)** surface layer (5 m), **(C, D)** middle layer (800 m), and **(E, F)** deep layer (2000 m). Black dashed lines in **(A)** indicate sections discussed in section 4.2.

TABLE 1 Comparison of defined parameters and areas of SCSMI.

Research	Definition parameters	Definition area
Xie et al. (1998)	Zonal wind, Outgoing longwave radiation	0 – 20 °N, 105 – 120°E
Yao and Qian (2001)	Moist potential vorticity	0 – 10°N, 105 – 120°E
Wang et al. (2004)	Zonal wind	3.75 – 16.25°N, 108.75 – 121.25°E
Jiang et al. (2006)	Black Body Temperature	10 – 20°N, 110 – 120°E
Mao (2008)	Potential Pseudo-equivalent Temperature, Zonal Wind	5 – 20°N, 110 – 120°E
This study	SCI_w (>0.9)	9 – 12°N, 112 – 117°E

surface circulation exhibits different features. Two low-value bands (SCI_o <0.4) are visible along the northern slope from the LS and across the basin from the middle east of Luzon Island. Conversely, high-value bands (SCI_o >0.7) are alternatively distributed from the northern shelf to the south. The values of SCI_o in the southern part of 12°N are generally larger than those in the NSCS, which indicates intensified seasonal variability in the SSCS (Liu et al., 2001). The maximum SCI_o over 0.9 corresponds to the maximum SCI_w in the southern central basin. The large values of surface SCI_o indicate the reversal of the surface ocean circulation. Additionally, Figure 3B depicts the magnitude of the reversed velocities, i.e., SCA_o. The high SCA_o over 0.9 m s^{-1} is concentrated on the western boundary near the Vietnam coast, signifying maximum velocity fluctuation in the SCS. As reported in previous studies, the strong

western boundary current along the Vietnam coast varies from southward in winter to northward in summer (Wang et al., 2013). The SCA_o is generally smaller than 0.2 m s^{-1} in the eastern part of the SCS basin, indicating a small amplitude of the seasonal cycle in the speed of the surface current in the eastern SCS.

Figures 2C, D depict the distribution of SCI_o and SCA_o in the middle layer at 800 m, respectively. SCI_o exhibits high values (>0.7) in the central and eastern SCS, while low-value (<0.5) bands appear in the northern and western SCS. The mean value of SCI_o at 800 m is 0.67, almost the same as at the surface (0.68), indicating that the seasonal cycle of the ocean circulation in the middle layer of the SCS is significant. However, SCA_o at the middle depth is one order of magnitude lower than that at the surface. The maximum SCA_o is only about 0.12 m s^{-1}, and high values over 0.08 m s^{-1} mainly appear

along the northern slope and the western boundary of the SCS basin, where SCI_o is lower than 0.5. High values of SCA_o do not necessarily appear in the same places as those of SCI_o because SCA_o depends only on the absolute vector departure from summer to winter. Still, SCI_o should be further divided by the local reference velocity. The distribution of low/high-value bands of SCI_o is opposite to that in the upper layer. In the deep layer at 2000 m (Figures 2E-F), the mean value of SCI_o is 0.52, and SCA_o continuously decreases to less than 0.025 m s^{-1} due to the decline of ocean current with depth. However, large values of SCI_o (>0.7) exist in all these three layers from the surface to the deep. The seasonal variation of the velocity vector remains strong even in the deep ocean. Unlike the strong seasonality of surface wind and ocean current in the SSCS, SCI_o has relatively low values in the middle and deep layers. Low SCI_o occupies a larger area in the NSCS in the surface layer, but the opposite situation appears in the middle and deep layers. The weak seasonal variation in the SSCS in deep circulation agrees with the conclusion of the previous study (Zhu et al., 2019).

4.2 Vertical distribution

To better understand the vertical distribution of SCI_o and SCA_o in the SCS, we have chosen three meridional sections and two zonal sections for analysis, as indicated by the dashed lines in Figure 2A. Section I corresponds to a meridional section along 120°E in the LS, and the corresponding SCI_o and SCA_o are shown in Figures 4A, B,

respectively. The distribution of SCI_o in this section is characterized by a three-layer structure, with low values (<0.2) at the top and bottom and high values (>0.8) at the middle depths. This is similar to the 'sandwiched' structure of zonal flows in the LS, as reported in previous studies (Tian et al., 2006). The northern section (>500 m) exhibits less seasonality, where the Kuroshio intrusion dominates. Strong seasonality is observed in the middle depths (500-1500 m), with high values of SCI_o concentrated in the southern part. In the deep layer (>1500 m), the seasonality is relatively weak. On the other hand, SCA_o shows a monotonic decrease from 0.4 m s^{-1} at the surface to 0.05 m s^{-1} at the bottom, with the highest value of 0.4 m s^{-1} found in the middle LS.

Figures 4C, D illustrate the vertical structures of SCI_o and SCA_o in Section II (along 118°E) across the SCS from south to north. SCI_o distribution (Figure 4C) displays vertical bands with alternating strong (>0.7) and weak (<0.5) values, with a width of approximately 100 km, which corresponds to the band-like pattern observed in the horizontal distribution of SCI_o in the upper ocean (Figure 3A). In the depths around 800 m, there is a layer of relatively high SCI_o values. High SCA_o values are concentrated in the upper ocean and decrease in magnitude with depth (Figure 4C). Four high-value cores with SCA_o >0.15 m s^{-1} appear near the surface at approximately 10°N, 15°N, 18°N, and 21°N.

To the west, Figures 4E, F display SCI_o and SCA_o in Section III (along 114°E) across the middle SCS, respectively. The SCI_o exhibits alternately strong and weak bands only in the NSCS north of 12°N, while high values above 0.6 dominate the upper 1000 m in the southern section, which corresponds to the horizontal distribution
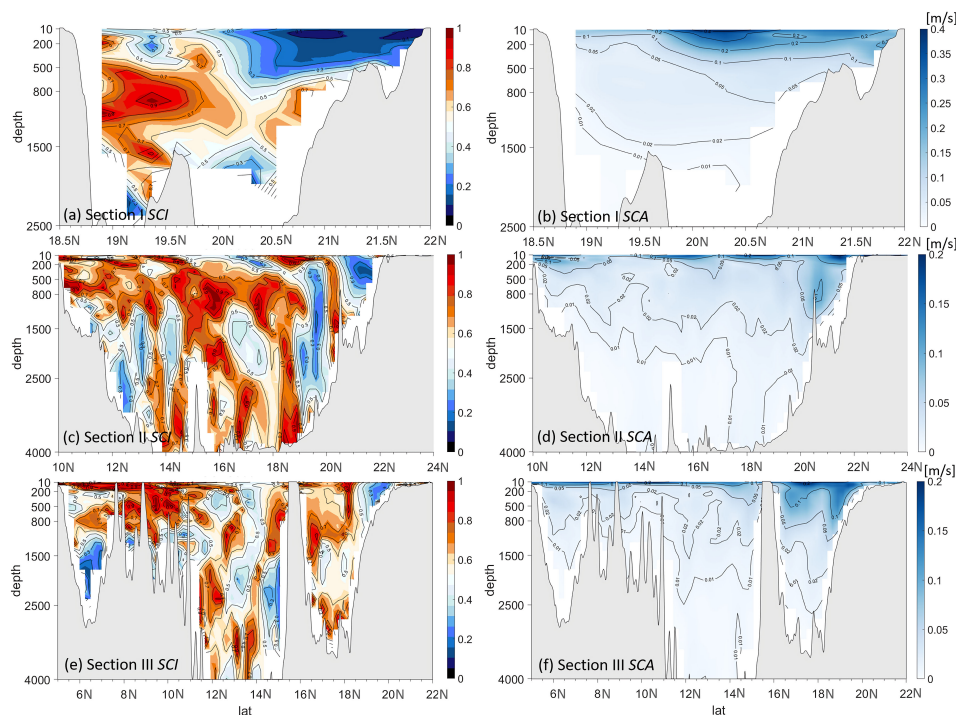

FIGURE 4
Distributions of SCI_o **(A, C, E)** and SCA_o **(B, D, F)** along meridional Sections I (120° E), II (118° E), and III (114° E) (dashed lines in Figure 3A). Gray shading denotes bottom topography.
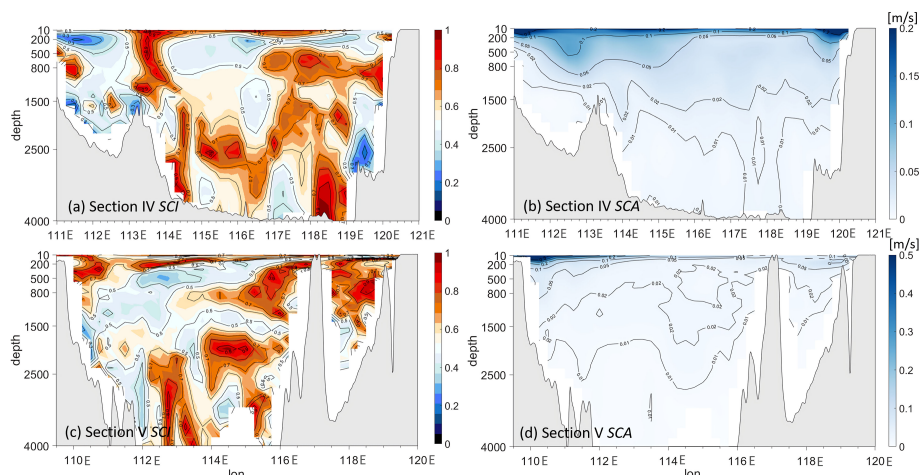
FIGURE 5

Vertical-zonal distributions of SCI_o (A, C) and SCA_o (B, D) along sections IV (18°N) and V (12°N) (dashed lines in Figure 3A). Gray shading denotes land and bottom topography.

shown in Figure 3. The distribution of SCA_o also displays differences between the north and SSCS, where large SCA_o values over 0.1 are limited to the upper 200 m south of 16°N and penetrate deeper than 500 m north of 16°N.

In Sections II and III, SCI_o values in the deep ocean below 2500 m are high, reaching values over 0.7 and even 0.9. This suggests a strong seasonality in the deep basin extending to the bottom.

Figure 5 displays the vertical distribution of SCI_o and SCA_o in zonal Sections IV (18°N) and V (12°N). In Section IV in the NSCS (Figure 5A), high SCI_o values (>0.7) and low SCI_o values (<0.5) alternate from west to east. The subsurface high-value bands are tightly concentrated at approximately 113.5°E and 118.5°E at all depths. In contrast, vast water between 200 m and 2000 m from 114°E to 117°E exhibits low values of SCI_o, indicating weak seasonality in the middle depths in the NSCS. In contrast, high SCI_o values still occur in the deepest basin below 2500 m from 118°E to 119°E, demonstrating strong seasonality in the deep basin. The vertical distribution of SCA_o (Figure 5B) shows a decaying pattern from top to bottom, with values greater than 0.1 m s^{-1} in the upper layer above 200 m. The deviation of the winter-summer current velocity reaches its maximum of about 0.2 m s^{-1} at the two ends of the section near Hainan Island and Luzon Island, respectively.

In the SSCS along Section V (Figures 5C, D), the SCI_o values are predominantly high (>0.7) in the upper 200 m, and they extend to 500 m near the Vietnam coast (west of 111°E). The corresponding SCA_o values are also high, with the most significant value exceeding 0.5 m s^{-1} near the surface. This high SCI_o and SCA_o in the region reveal a strong seasonal reversed western boundary current along the Vietnam coast. The vertical distribution of SCI_o and SCA_o suggests that the boundary current extends to as deep as 500 m, consistent with a previous study (Zu et al., 2020). In the middle depths between 500 m and 2000 m, the seasonality of the current is distinctly different in the western and eastern basins on two sides of 114°E, with low SCI_o (<0.5) appearing on the west and SCI_o >0.7 on

the east. Once again, the SCI_o values are high (>0.7) and even 0.9 in the deep basin below 2500 m, indicating strong seasonality in the deep basin down to the bottom.
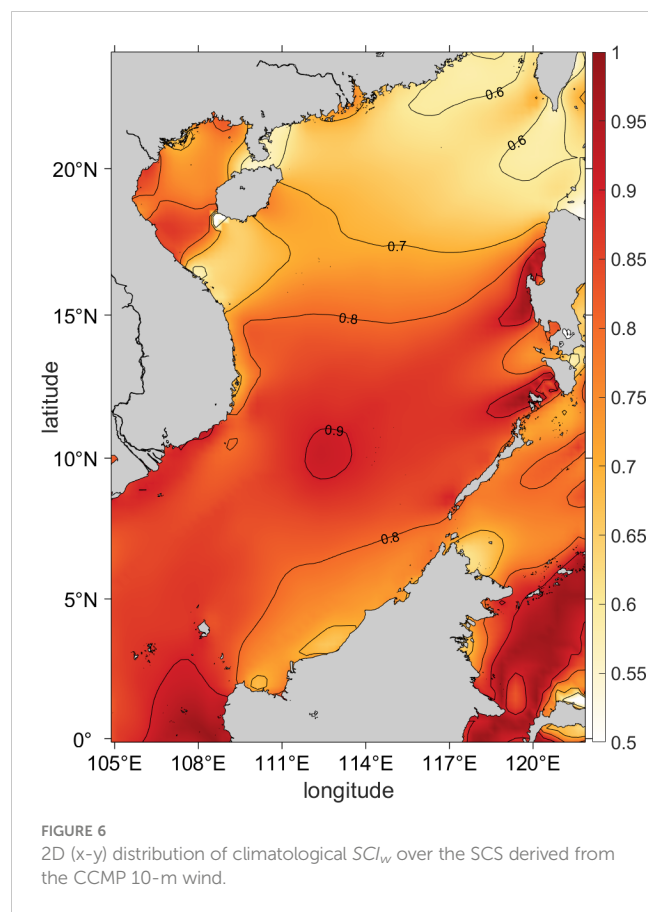

FIGURE 6

2D (x-y) distribution of climatological SCI_w over the SCS derived from the CCMP 10-m wind.
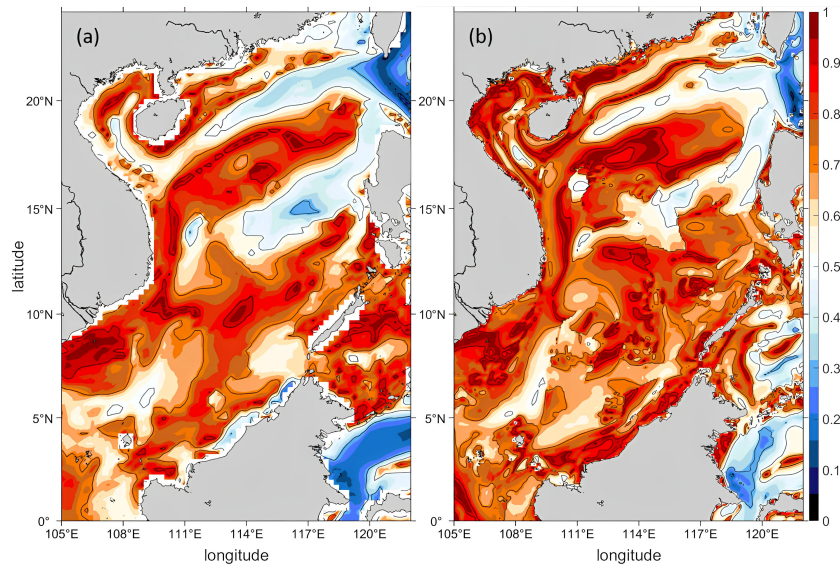
FIGURE 7
2D (x-y) distribution of climatological surface SCI_o in the SCS derived from SODA surface velocity **(A)** and GLORYS12V1 surface velocity **(B)**.

5 Discussion

5.1 About the datasets

In this study, we use the ERA5 wind data and SODA current data for the SCI analysis. Here, we use the Cross-Calibrated Multi-Platform (CCMP) monthly wind data (https://data.remss.com/ccmp/v03.0/monthly/) and the high-resolution Global Ocean Physics Reanalysis (GLORYS12V1) ocean current data (https://data.marine.copernicus.eu/product/GLOBAL_MULTIYEAR_PHY_001_030/download?dataset=cmems_mod_glo_phy_my_0.083_P1M-m) for comparison.

The CCMP wind data has a horizontal resolution of 0.25°, and covers the period from 1994 to 2019. Figure 6 shows the 2D (x-y) distribution of SCI_w over the SCS calculated from the CCMP climatological 10-m wind. One can see that it has similar values and distribution pattern with that from ERA5 wind data (Figure 2E). High values of SCI_w over 0.8 covers the similar region south of 15°N as that from the EAR5 data, although the extreme-value area over 0.9 from the CCMP data is a little smaller than that from ERA5. The spatial correlation coefficient between the climatological SCI_w from the two datasets reaches 0.81.

The GLORYS12V1 ocean current data has a horizontal resolution of 1/12° and covers the period from 1993 to 2020. Figures 7A, B show the surface climatological SCI_o in the SCS calculated from the SODA data and the GLORYS12V1 data, respectively. One can see that the whole pattern and values of SCI_o from GLORYS12V1 data are close to that from SODA data although small-scale details appeared in the GLORYS12V1 data. The band-like pattern with alternating high and low bands distributed from north to south are both significant in the two datasets. The finer resolution impacts little to the SCI_o results.
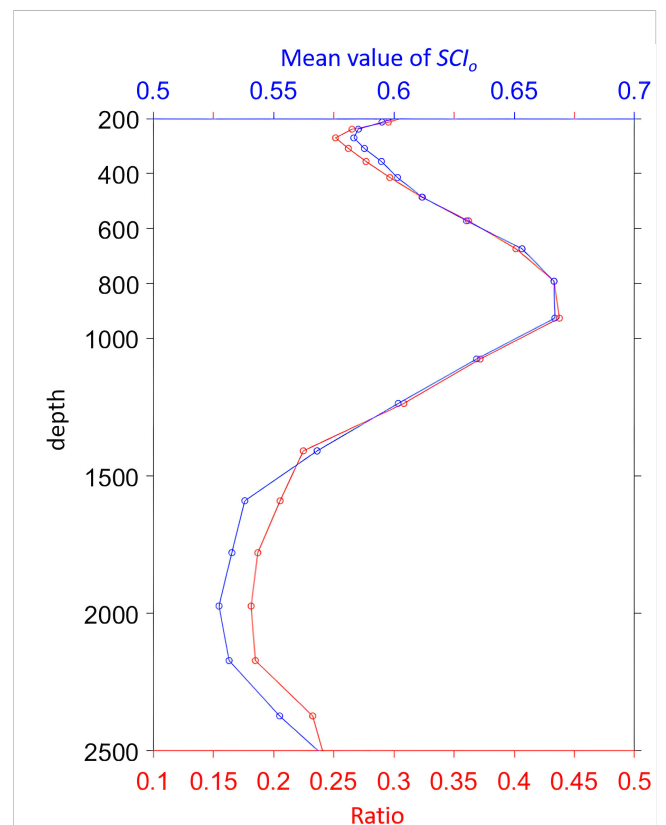

FIGURE 8
Vertical profiles of the mean value of SCI_o (blue line) and the ratio of the area with SCI_o >0.7 to the total area in each layer (red line).
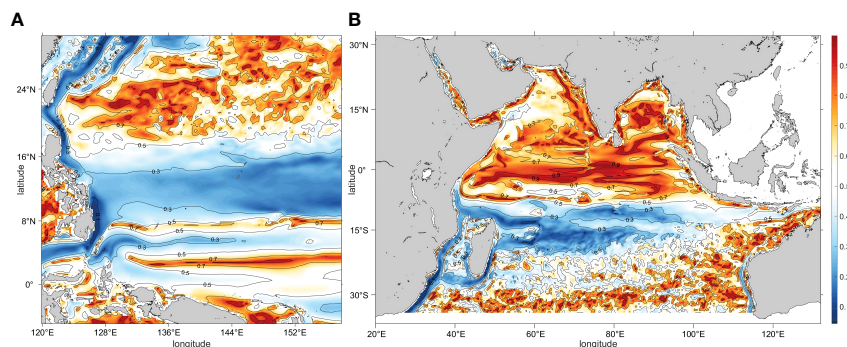
FIGURE 9
2D (x–y) distribution of climatological SCI_o over the west Pacific Ocean **(A)** and India Ocean **(B)** calculated from the surface velocity from SODA data.

5.2 Seasonal variation of the deep-layer circulation in the SCS

As noted in Section 4.1, the average SCI_o at a depth of 800 m is nearly identical to that at the surface and has a high value of 0.67. We further investigated the increased seasonality in the middle layer. As depicted in Figure 8, the mean SCI_o profile forms a reversed "S" shape, with three local maxima of 0.68, 0.67, and 0.52 at the surface, 800 m, and 2500 m, respectively, and two local minima of 0.57 and 0.52 at 300 m and 2000 m, respectively. The values are all above 0.65 in the middle depths from 800 m to 1000 m, indicating a strong seasonality in the middle layer. Additionally, the ratio of the area with high SCI_o (>0.7) to the total area peaks at 42% in the middle layer, providing further evidence of the middle-layer enhancement of seasonality. Previous studies suggested a three-layer circulation in the SCS (Gan et al., 2016; Cai et al., 2020; Zhu et al., 2022) and proposed the combined effects of wind and inflow through the LS are the primary mechanism. The increase of SCI_o at depths of 800-1000 m in the northern part of the LS (Figure 3A) suggests that the seasonal exchange between the SCS and the Pacific Ocean may contribute to the strong seasonality in the middle layer of the SCS.

The new indexes introduced in this study provide valuable insights into the deep circulation of the SCS. In previous research, the deep circulation was believed to be cyclonic with slight seasonal variation, primarily controlled by the overflow from the LS and influenced by topography (Yuan, 2022). However, the large values of SCI_o observed in this study suggest a significant and strong seasonality in the deep circulation. Numerical modeling by Lan et al. (2015) showed a strong basin-scale cyclonic gyre in summer that was almost unidentifiable in winter in the deep SCS. Tang et al. (2022) also proposed seasonal variability of deep circulation based on a two-level nested model, indicating a basin-scale cyclonic circulation with a strong southward boundary current in summer and a northeast-southwest throughflow pattern without a west boundary current in winter. The SCI_o serves as a quantitative index for the seasonal variation of the deep circulation and may be linked to the heaving of isopycnal surfaces in the upper layer due to seasonal varying Ekman pumping induced by the reversed wind curl over the SCS, as noted by Tan et al. (2015) and Han (2021).

5.3 Application of SCI_o in the open ocean

The SCI provides an index to quantify the seasonal ocean circulation not only in the marginal seas but also the open oceans. As shown in Figure 9, SCI_o is applied in open oceans such as the west Pacific Ocean (WPO) and the India Ocean (IO). One can see a clear low-value strip (SCI_o<0.3) distributed in the North Equatorial Current (NEC) (8-16°N) and branches northward and southward along the western boundary in the Kuroshio and Mindanao currents in the WPO (Figure 9A), indicating relatively stable current direction of the western boundary current system. On the other hand, strong seasonal variations with SCI_o over 0.7 appear in the subtropical area from 18°N to 28°N, where mesoscale eddies are active with significant seasonal variation (Qiu and Chen, 2013). In the equatorial area, SCI_o reaches 0.8 in the Northern Equatorial Counter Current (NECC) near 8°N and the Southern Equatorial Current (SEC) near 3°N, consistent with previous research of the seasonal variation (Hsin and Qiu, 2012).

In the IO (Figure 9B), high values of SCI_o over 0.70 occupy most area of the northern IO, clearly showing the seasonal circulation under the impact of the Indian Ocean monsoon (Yim et al., 2014). In the southern IO (south of 5°S), low SCI_o below 0.30 appears in the western tropic area between 20°S and 5°S and near the western boundary, while SCI_o over 0.5 appears in the eastern ocean near west Australian where the west Australia current has evident seasonality (Schott et al., 2009).

6 Conclusion

This study introduces two new indexes, SCI and SCA, which allow for quantifying seasonal variation in the ocean circulation. We apply these indexes to the SCS, a region heavily influenced by monsoon winds. The SCI_w accurately represents the distribution of the monsoon winds over the SCS, effectively quantifies the intensity of the SCSM, and identifies critical areas for the SCSMI calculations. The SCI_o reveals the pattern of seasonal circulation in the upper SCS and shows apparent north-south asymmetry in seasonality, with SCI_o in the southern SCS generally 20% higher than in the northern SCS. The SCI_o in the upper layer also displays a band-like pattern

with alternating high and low bands distributed from north to south. The southwest-northeastward alternating bands are more pronounced in the central and eastern SCS, possibly due to westward long Rossby waves initiated from the east boundary and related Rossby normal modes in the semi-closed basin. High values of SCI_o and SCA_o near the surface accurately indicate the presence of the western boundary current near the Vietnam coast. In the middle and deep layer, the SCI_o show unexpected high values over 0.7 in most basin areas, implying strong seasonality in the deep SCS. The application of SCI in other ocean area and quantified analysis with other phenomena worth further pursuing.

Data availability statement

The original contributions presented in the study are included in the article/supplementary material. Further inquiries can be directed to the corresponding author.

Author contributions

QL: data analysis; writing—original draft. RXH: concepts discussed; writing—review and editing. LX: study design; writing — review and editing. All authors have read and agreed to the published version of the manuscript.

Conflict of interest

The authors declare that the research was conducted in the absence of any commercial or financial relationships that could be construed as a potential conflict of interest.

Publisher's note

All claims expressed in this article are solely those of the authors and do not necessarily represent those of their affiliated organizations, or those of the publisher, the editors and the reviewers. Any product that may be evaluated in this article, or claim that may be made by its manufacturer, is not guaranteed or endorsed by the publisher.

References

Cai, Z., Gan, J., Liu, Z., Hui, C. R., and Li, J. (2020). Progress on the formation dynamics of the layered circulation in the south China Sea. *Prog. Oceanogr.* 181, 102246. doi: 10.1016/j.pocean.2019.102246

Fang, G., Wang, G., Fang, Y., and Fang, W. (2012). A review on the south China Sea western boundary current. *Acta Oceanol. Sin.* 31, 1–10. doi: 10.1007/s13131-012-0231-y

Gan, J., Liu, Z., and Hui, C. R. (2016). A three-layer alternating spinning circulation in the south China Sea. *J. Phys. Oceanogr.* 46, 2309–2315. doi: 10.1175/JPO-D-16-0044.1

Han, L. (2021). The sloshing and diapycnal meridional overturning circulations in the Indian ocean. *J. Phys. Oceanogr.* 51, 701–725. doi: 10.1175/JPO-D-20-0211.1

He, C., Zhou, W., Li, T., Zhou, T., and Wang, Y. (2022). East Asian Summer monsoon enhanced by COVID-19. *Clim. Dyn.* 59, 2965–2978. doi: 10.1007/s00382-022-06247-8

Hsin, Y. C., and Qiu, B. (2012). Seasonal fluctuations of the surface north equatorial countercurrent (NECC) across the pacific basin. *J. Geophys. Res.* 117 (C6). doi: 10.1029/2011JC007794

Hu, J., Ho, C.-R., Xie, L., and Zheng, Q. (2020). *Regional oceanography of the south China Sea* (Singapore: World Scientific). 43–75. doi: 10.1142/9789811206917_0003

Hu, J., Kawamura, H., Hong, H., and Qi, Y. (2000). A review on the currents in the south China Sea: seasonal circulation, south China Sea warm current and kuroshio intrusion. *J. Oceanogr.* 56, 607–624. doi: 10.1023/A:1011117531252

Jiang, J., Qin, D., and Liu, C. (2006). A preliminary study of the south China Sea and East Asian summer monsoon indices based on satellite observations. *J. Trop. Metorology* 22, 423–430. doi: 10.3969/j.issn.1004-4965.2006.05.002

Kajikawa, Y., and Wang, B. (2012). Interdecadal change of the south China Sea summer monsoon onset. *J. Climate* 25, 3207–3218. doi: 10.1175/JCLI-D-11-00207.1

Lan, J., Wang, Y., Cui, F., and Zhang, N. (2015). Seasonal variation in the south China Sea deep circulation. *J. Geophys. Res.* 120, 1682–1690. doi: 10.1002/2014JC010413

Liu, Q., Kaneko, A., and Jilan, S. (2008). Recent progress in studies of the south China Sea circulation. *J. Oceanogr.* 64, 753–762. doi: 10.1007/s10872-008-0063-8

Liu, G., and Lan, J. (2022). Distribution of seasonal signals in the deep south China Sea. *Deep Sea Res. Part I Oceanogr. Res. Pap.* 190, 103895. doi: 10.1016/j.dsr.2022.103895

Liu, Z., Yang, H., and Liu, Q. (2001). Regional dynamics of seasonal variability in the south China Sea. *J. Phys. Oceanogr.* 31, 272–284. doi: 10.1175/1520-0485(2001)031<0272:RDOSVI>2.0.CO;2

Liu, X., and Zhou, H. (2020). Seasonal variations of the north equatorial current across the pacific ocean. *J. Geophys. Res.* 125, e2019JC015895. doi: 10.1029/2019JC015895

Liu, B., and Zhu, C. (2021). Subseasonal-to-Seasonal predictability of onset dates of south China Sea summer monsoon: a perspective of meridional temperature gradient. *J. Climate* 34, 5601–5616. doi: 10.1175/JCLI-D-20-0696.1

Mao, J., and Wu, G. (2007). Interannual variability in the onset of the summer monsoon over the Eastern bay of Bengal. *Theor. Appl. Climatol.* 89, 155–170. doi: 10.1007/s00704-006-0265-1

Mao. (2008). The interannual anomalies of the onset of the South China Sea summer monsoon and the Indian summer monsoon. *[master's thesis]*. (Nanjing: Nanjing University of Information Science and Technology).

Phillips, H. E., Tandon, A., Furue, R., Hood, R., Ummenhofer, C. C., Benthuysen, J. A., et al. (2021). Progress in understanding of Indian ocean circulation, variability, air–sea exchange, and impacts on biogeochemistry. *Ocean Sci.* 17, 1677–1751. doi: 10.5194/os-17-1677-2021

Qiu, B., and Chen, S. (20132013). Concurrent decadal mesoscale eddy modulations in the western north pacific subtropical gyre. *J. Phys. Oceanogr.* 43 (2), 344–358. doi: 10.1175/JPO-D-12-0133.1

Qu, T., Du, Y., and Sasaki, H. (2006). South China Sea throughflow: a heat and freshwater conveyor. *Geophys. Res. Lett.* 33, L23617. doi: 10.1029/2006GL028350

Schott, F. A., Xie, S. P., and McCreary, J. P. (2009). Indian Ocean circulation and climate variability[J]. *Rev. Geophysics* 47 (1). doi: 10.1029/2007RG000245

Tan, W., Huang, R. X., Wang, W., and Wang, X. (2015). Zonal overturning circulation and heat flux induced by heaving modes in the world oceans. *Acta Oceanol. Sin.* 34, 80–91. doi: 10.1007/s13131-015-0751-3

Tang, S., Chen, X., Zeng, Z., and Liu, X. (2022). Numerical investigation of the south China Sea deep circulation. *Acta Oceanol. Sin.* 41, 1–11. doi: 10.1007/s13131-021-1879-y

Tian, J., and Qu, T. (2012). Advances in research on the deep south China Sea circulation. *Chin. Sci. Bull.* 57, 3115–3120. doi: 10.1007/s11434-012-5269-x

Tian, J., Yang, Q., Liang, X., Xie, L., Hu, D., Wang, F., et al. (2006). Observation of Luzon strait transport. *Geophys. Res. Lett.* 33, L19607. doi: 10.1029/2006GL026272

Wang, B., Huang, F., Wu, Z., Yang, J., Fu, X., and Kikuchi, K. (2009). Multi-scale climate variability of the south China Sea monsoon: a review. *Dynam. Atmos. Oceans* 47, 15–37. doi: 10.1016/j.dynatmoce.2008.09.004

Wang, D., Liu, Q., Huang, R. X., Du, Y., and Qu, T. (2006). Interannual variability of the south China Sea throughflow inferred from wind data and an ocean data assimilation product. *Geophys. Res. Lett.* 33, L14605. doi: 10.1029/2006GL026316

Wang, D., Liu, Q., Xie, Q., He, Z., Zhuang, W., Shu, Y., et al. (2013). Progress of regional oceanography study associated with western boundary current in the south China Sea. *Chin. Sci. Bull.* 58, 1205–1215. doi: 10.1007/s11434-012-5663-4

Wang, D., Wang, W., Shi, P., Guo, P., and Gan, Z. (2003). Establishment and adjustment of monsoon-driven circulation in the south China Sea. *Sci. China Ser. D-Earth Sci.* 46, 173–181. doi: 10.1360/03yd9016

Wang, G., Xie, S. P., Qu, T., and Huang, R. X. (2011). Deep south China Sea circulation. *Geophys. Res. Lett.* 38, L05601. doi: 10.1029/2010GL046626

Wang, B., Zhang, Y., and Lu, M. M. (2004). Definition of south China Sea monsoon onset and commencement of the East Asia summer monsoon. *J. Climate* 17, 699–710. doi: 10.1175/2932.1

Wei, Z., Li, S., Susanto, R. D., Wang, Y., Fan, B., Xu, T., et al. (2019). An overview of 10-year observation of the south China Sea branch of the pacific to Indian ocean throughflow at the karimata strait. *Acta Oceanol. Sin.* 38, 1–11. doi: 10.1007/s13131-019-1410-x

Wyrtki, K. (1961). *Physical oceanography of the southeast Asian waters* Vol. 2 (California, United States: University of California, Scripps Institution of Oceanography).

Xie, A., Chung, Y. S., Liu, X., and Ye, Q. (1998). The interannual variations of the summer monsoon onset over the south China Sea. *Theor. Appl. Climatol.* 59, 201–213. doi: 10.1007/s007040050024

Xie, L., Zheng, Q., Tian, J., Zhang, S., Feng, Y., and Yi, X. (2016). Cruise observation of rossby waves with finite wavelengths propagating from the pacific to the south China Sea. *J. Phys. Oceanogr.* 46, 2897–2913. doi: 10.1175/JPO-D-16-0071.1

Yao, Y., and Qian, Y. (2001). A study on the southwest monsoon index of the south china sea defined by moist potential vorticity and its relationship with regional precipitation in China. *J. Nanjing University: Natural Sci.* 37, 781–788.

Yim, S. Y., Wang, B., Liu, J., and Wu, Z. (2014). A comparison of regional monsoon variability using monsoon indices. *Clim. Dyn.* 43, 1423–1437. doi: 10.1007/s00382-013-1956-9

Yuan, D. (2002). A numerical study of the south China Sea deep circulation and its relation to the Luzon strait transport. *Acta Oceanol. Sin.* 2, 187–202.

Zheng, Q., Tai, C. K., Hu, J., Lin, H., Zhang, R. H., Su, F. C., et al. (2011). Satellite altimeter observations of nonlinear rossby eddy–kuroshio interaction at the Luzon strait. *J. Oceanogr.* 67, 365–376. doi: 10.1007/s10872-011-0035-2

Zhou, T., Wu, B., Guo, Z., He, C., Zou, L., Chen, X., et al. (2018). A review of East Asian summer monsoon simulation and projection: achievements and problems, opportunities and challenges. *Chin. J. Atmos Sci.* 42, 902–934. doi: 10.3878/j.issn.1006-9895.1802.17306

Zhu, Y., Cao, G., Wang, Y., Li, S., Xu, T., Wang, D., et al. (2022). Variability of the deep south China Sea circulation derived from HYCOM reanalysis data. *Acta Oceanol. Sin.* 41, 54–64. doi: 10.1007/s13131-021-1952-6

Zhu, Y., Sun, J., Wang, Y., Li, S., Xu, T., Wei, Z., et al. (2019). Overview of the multi-layer circulation in the south China Sea. *Prog. Oceanogr.* 175, 171–182. doi: 10.1016/j.pocean.2019.04.001

Zu, T., Wang, D., Wang, Q., et al. (2020). A revisit of the interannual variation of the South China Sea upper layer circulation in summer: correlation between the eastward jet and northward branch. *Clim. Dyn.* 54, 457–471. doi: 10.1007/s00382-019-05007-5